Precambrian Research 373 (2022) 106646

Contents lists available at ScienceDirect

Precambrian Research

journal homepage: www.elsevier.com/locate/precamres

Mercury isotopic compositions of the Precambrian rocks and implications for tracing mercury cycling in Earth's interior

Changzhou Deng [a], Hongyan Geng [b], Tingting Xiao [c], Di Chen [a], Guangyi Sun [d], Runsheng Yin [a,*]

[a] State Key Laboratory of Ore Deposit Geochemistry, Institute of Geochemistry, Chinese Academy of Sciences, Guiyang 550081, China
[b] Science Unit, Lingnan University, Hong Kong, China
[c] College of Earth Science, Jilin University, Changchun 130061, China
[d] State Key Laboratory of Environment Geochemistry, Institute of Geochemistry, Chinese Academy of Sciences, Guiyang 550081, China

ARTICLE INFO

Keywords:
Precambrian basement
Metamorphism
Hg isotope
Mass-independent fractionation
Material cycling

ABSTRACT

Mercury isotopes undergo unique mass-independent fractionation (MIF) during photochemical processes on Earth's surface. Studies have observed pronounced Hg-MIF signals in sedimentary and magmatic rocks, suggesting recycling of Hg from Earth's surface systems into the lithosphere via sedimentation and magmatism. However, the isotopic signature of Hg in metamorphic rocks and the geochemical fate of Hg during metamorphism remain unclear. Precambrian basements are important components of cratons or orogenic belts on Earth. Here, we study the Hg concentration and isotopic composition of Precambrian metamorphic and sedimentary rocks from the eastern Central Asian Orogenic Belt, and North and South China cratons. Metamorphic rocks show much lower Hg contents (0.21–7.8 ppb) than sedimentary rocks (2.6–694 ppb), indicating a substantial loss of Hg during metamorphism. The lack of correlation between δ^{202}Hg values (–2.41 to 0.18‰) and metamorphic grades indicates no systematic mass-dependent fractionation (MDF) of Hg isotopes during metamorphism. The Δ^{199}Hg/Δ^{201}Hg ratios of ~ 1.0 for both metamorphic and sedimentary rocks indicate Hg was sourced from Earth's surface systems. The coupling of Hg-MIF signals between the metasedimentary rocks and the sedimentary settings of their protolith suggests no Hg-MIF during metamorphism. The negative Δ^{199}Hg values (–0.30 to –0.02‰) in the Precambrian coastal sedimentary rocks imply the input of Hg into coastal regions via soil erosion. The positive Δ^{199}Hg values (0.06 to 0.31‰) in the Precambrian marine sedimentary rocks suggest deposition of atmospheric Hg(II) to open oceans via wet deposition. The lack of significant Hg-MIF during metamorphism and other underground geological processes shows that Hg-MIF signals can work as a reliable tracer for indicating material cycling in Earth's interior.

1. Introduction

Mercury's seven isotopes (196, 198–202, 204, amu) undergo significant mass-dependent fractionation (usually defined as δ^{202}Hg) and mass-independent fractionation (usually defined as Δ^{199}Hg) during their cycling in the environment (Bergquist and Blum, 2007; Blum et al., 2014). Hg-MDF ubiquitously occurs during various geochemical and biological processes, resulting in a large δ^{202}Hg variation of ~ 10‰ in natural samples (Blum et al., 2014 and references therein). Hg-MIF in natural samples occurs mainly via Hg(II) photoreduction on Earth's surface (Bergquist and Blum, 2007). The primitive mantle lacks Hg-MIF signals (Δ^{199}Hg of ~ 0‰, Sherman et al., 2009; Moynier et al., 2021), whereas marine (seawater, halobios and sediments) and terrestrial systems (soil and plants) show opposing Hg-MIF signals with Δ^{199}Hg of > 0‰ and < 0‰, respectively (Sonke, 2011; Blum et al., 2014). Previous studies based on the "δ^{202}Hg-Δ^{199}Hg" two-dimensional signals in sedimentary rocks and sulfide minerals have provided important constraints on Hg sources in modern- and paleo-environments (Gratz et al., 2010; Sherman et al., 2012; Blum et al., 2014; Chen et al., 2016; Grasby et al., 2017; Shen et al., 2020, 2022; Zhou et al., 2021) and metal sources in hydrothermal deposits (Tang et al., 2017; Xu et al., 2018; Yin et al., 2019; Fu et al., 2020; Deng et al., 2021a, 2021b). Recent studies on Hg isotopes igneous rocks demonstrated that magmatic processes do not induce Hg-MIF, enabling its potential use to distinguish magma sources, especially for tracing crustal recycling into the mantle (Moynier et al., 2021; Wang et al., 2021; Yin et al., 2022).

* Corresponding author.
E-mail address: yinrunsheng@mail.gyig.ac.cn (R. Yin).

https://doi.org/10.1016/j.precamres.2022.106646
Received 26 January 2022; Received in revised form 14 March 2022; Accepted 15 March 2022
Available online 21 March 2022

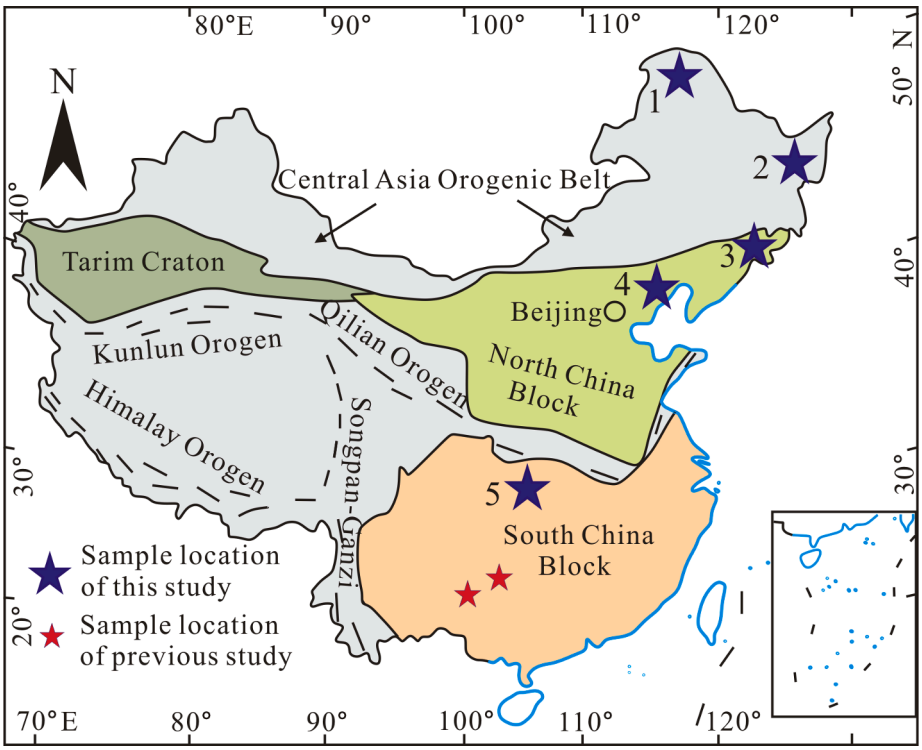

Fig. 1. Simplified geological map showing the sampling locations (after Zheng et al., 2013).

The Precambrian basements consisting of metamorphosed and un-metamorphosed sedimentary rocks are important components of cratons and orogens around the world. These rocks record key information for Earth's early-stage tectonic and environment evolution (e.g., Condie, 1990; Bauluz et al., 2000; Zhao et al., 2004, 2005; Dasgupta et al., 2008; Ader et al., 2016; Long et al., 2019; Ward et al., 2019; Zhou et al., 2021), and are important campaigner during the crust-mantle interaction, given their closer adhesion to the mantle or juvenile lower crust than the Phanerozoic rocks. However, the isotope fractionation of Hg during metamorphic processes is yet not developed. A study of Hg isotopic compositions on the Precambrian basements will provide key insights into (1) the mechanism of Hg isotope fractionation during metamorphism; (2) the geochemical fate of Hg in the Precambrian era when the atmosphere-land–ocean system was much different from the Phanerozoic.

Here we investigate the Hg isotopic composition of metamorphosed and un-metamorphosed Precambrian sedimentary rocks from the eastern Central Asian Orogenic Belt (CAOB), South and North China cratons. In the three areas, we observe similar Δ^{199}Hg values between the equivalent metamorphosed and un-metamorphosed sedimentary rocks, which suggests limited Hg-MIF during metamorphism.

2. Samples and geological backgrounds

The Precambrian metamorphosed sedimentary rocks (e.g., gneiss, schist, slate) were collected at three sites in China (Fig. 1). Specifically, two mica schist and eight biotite plagioclase gneiss samples were collected from the Neoproterozoic Xinghuadukou Group in the Erguna Block, eastern CAOB, NE China (Fig. 1, location No. 1). Protoliths of these rocks are Al-rich pelites, which were formed at the active continental margin setting (Miao et al., 2008; Wu et al., 2012; Xu, 2018); Eight graphite schist samples were collected from the Meso-Neoproterozoic Mashan Group in the Jiamusi Block, eastern CAOB (Fig. 1, location No. 2). Protoliths of the graphite schist are organic carbon-enriched pelite formed at the stable sea basin (Li et al., 2008); In the north margin of the North China Craton, two biotite gneisses and four sandy slates were sampled from the Archean Jiapigou and the Mesoproterozoic Seluohe groups, respectively (Fig. 1, location No. 3). The Jiapigou Group consist of supracrustal rocks, protolith of which were formed at the continental margin setting (BGMRJP, 1988). The Seluohe Group is composed of metavolcanic-clastic rocks, metasandstone, slate, mica schist and carbonates (Li et al., 2007). Components of metasandstone and sandy slate in the Seluohe Group indicate a shallow-water sedimentary setting.

The Precambrian un-metamorphosed sedimentary rocks (e.g., carbonate, siltstone and shales) were collected at two sites in China (Fig. 1). Specifically, four limestone and dolostone samples were collected from the Mesoproterozoic Gaoyuzhuang Formation in the northern North China Craton (Fig. 1, location No. 4). The Gaoyuzhuang Formation mainly consists of carbonates, representing shallow-water platform deposition (BGMRHP, 1989); Nineteen black shale, limestone, and dolostone samples were collected from the Neoproterozoic Dengying, Doushantuo and Nantuo formations in the Jiulongwan section of the Yangtze Block (Fig. 1, location No. 5), South China. These formations represent shelf to basinal deposition settings (McFadden et al., 2008).

3. Analytical methods

All the collected samples are fresh rocks without any hydrothermal alteration or mineralization. After removing their surface, the samples were air-dried, crushed, and powdered to 200 mesh, prior to chemical analyses. Total Hg (THg) contents of the samples were measured using a DMA-80 Hg analyzer (Hg detection limit: 0.01 ng/g) at the Institute of Geochemistry, Chinese Academy of Sciences (IGCAS). Measurements of standard reference material (GSS-4, soil) yielded THg recoveries of 95–110%. Triplicate analyses for selected samples show uncertainty (2SD) of $< 10\%$ for THg.

An approximate amount of samples containing 10 ng of Hg were weighed and prepared using the double-stage thermal combustion and pre-concentration protocol for Hg isotope analyses (Zerkle et al., 2020). Standard reference material (GSS-4, soil) was prepared in the same way as the samples, yielding Hg recoveries of 90–100%. Method blanks were

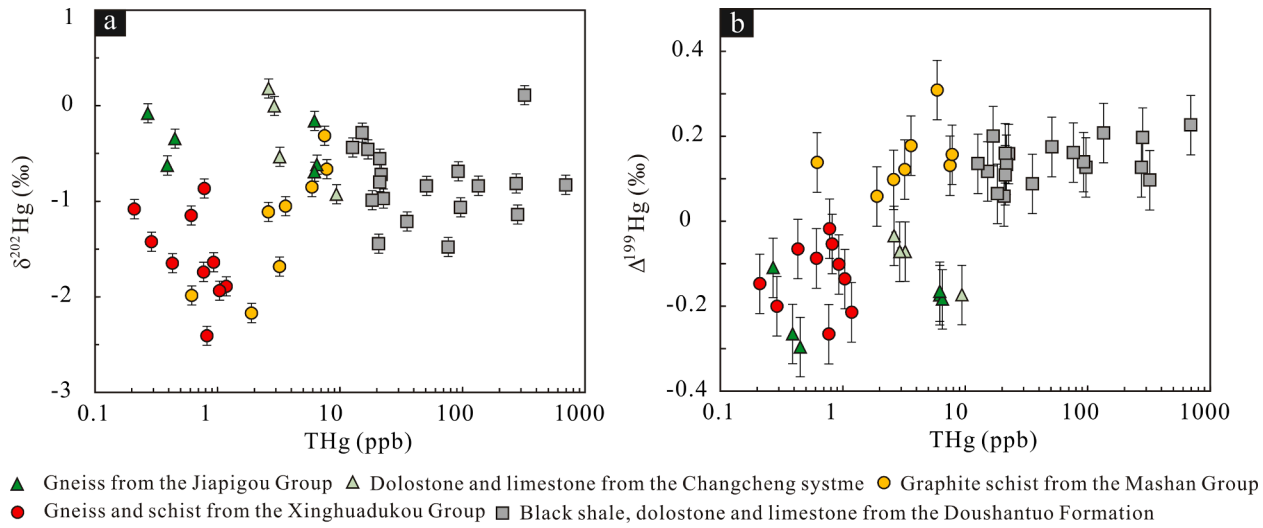

Fig. 2. (a) THg vs. δ^{202}Hg and (b) THg vs. Δ^{199}Hg diagrams.

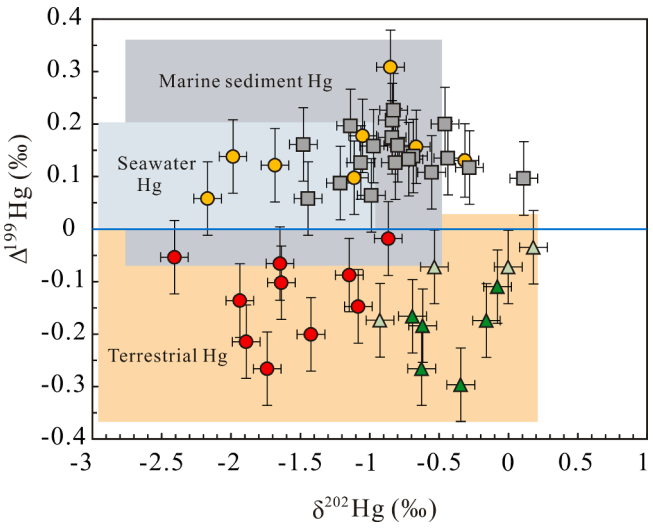

Fig. 3. Δ^{199}Hg versus δ^{202}Hg diagram for the studied Precambrian samples in China (after Deng et al. 2021a and reference therein). Area of terrestrial Hg is defined by Blum et al. (2014, and references therein), marine sediments Hg is that defined by Yin et al. (2015) and Meng et al. (2019), and seawater Hg as defined by Štrok et al. (2015). Legends are the same as in Fig. 2.

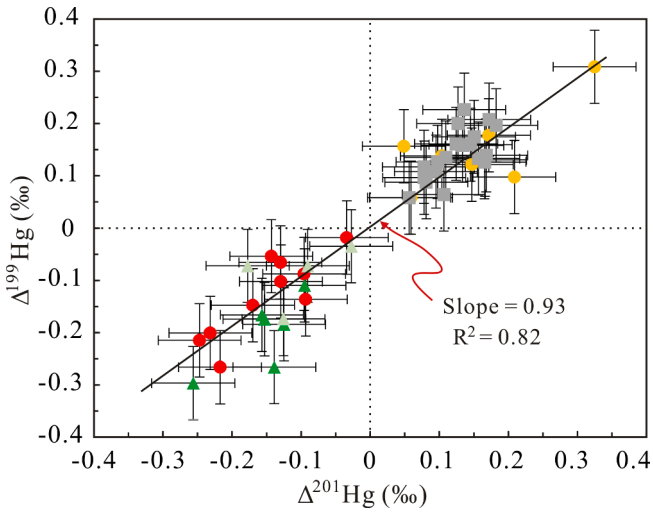

Fig. 4. Δ^{199}Hg versus Δ^{201}Hg diagram for the studied Precambrian samples in China. Legends are the same as in Fig. 2.

also prepared, which show Hg concentrations lower than the detection limit, precluding the lab contamination. The preconcentrated solutions (~10 ng Hg in 5 mL of 40% reverse aqua regia solution) were diluted to 0.5 ng/mL Hg, and were measured using a Neptune Plus multi-collector inductively-coupled plasma mass spectrometer at IGCAS, following a previous method (Yin et al., 2016). The Hg concentration in the acid blanks was lower than 50 pg/mL. Hg-MDF is expressed in δ^{202}Hg notation in units of ‰ referenced to the NIST-3133 Hg standard (analyzed before and after each sample):

$$\delta^{202}Hg(‰) = [(^{202}Hg/^{198}Hg_{sample})/(^{202}Hg/^{198}Hg_{standard}) - 1] \times 1000$$

MIF is reported in Δ notation, which describes the difference between the measured δ^{xxx}Hg and the theoretically predicted δ^{xxx}Hg value, in units of ‰:

$$\Delta^{xxx}Hg = \delta^{xxx}Hg - \delta^{202}Hg \times \beta$$

XXX = 199, 200, and 201. β is 0.2520 for ^{199}Hg, 0.5024 for ^{200}Hg, and 0.7520 for ^{201}Hg (Blum and Bergquist, 2007). NIST-3177 secondary standard solutions, dilluted in 0.5 ng/mL in 10% HCl, were measured in every 6 samples. The overall average and uncertainty of NIST-3177 (δ^{202}Hg: –0.57 ± 0.10‰; Δ^{199}Hg: –0.02 ± 0.07‰; Δ^{201}Hg: –0.03 ± 0.06‰, 2SD, n = 8) and GSS-4 (δ^{202}Hg: –1.71 ± 0.04‰; Δ^{199}Hg: –0.38 ± 0.06‰; Δ^{201}Hg: –0.35 ± 0.02‰, 2SD, n = 3) agrees well with previous studies (Blum and Berquist, 2007). Uncertainties of δ^{202}Hg, Δ^{199}Hg and Δ^{201}Hg reported here correspond to the 2SD values of NIST-3177.

4. Results

THg contents and Hg isotopic compositions of the studied samples are given in Supplementary Table S1. The rocks have an overall range of THg contents of 0.21–694 ppb (Fig. 2). Specifically, metamorphic rocks from the Xinghuadukou, Jiapigou, Mashan and Seluohe groups have low THg concentrations (0.21–7.80 ppb), whereas sedimentary rocks from the Gaoyuzhuang and Doushantuo Formations have much higher THg concentrations (2.60–694 ppb).

The studied samples have δ^{202}Hg values ranging from –2.41 to 0.18‰, which show no correlation with THg contents and metamorphic grades (Fig. 2**a**). They show a large variation of Δ^{199}Hg (–0.30 to 0.31‰, Fig. 2**b**) that is 9 times the analytical uncertainty (±0.07‰). The gneiss

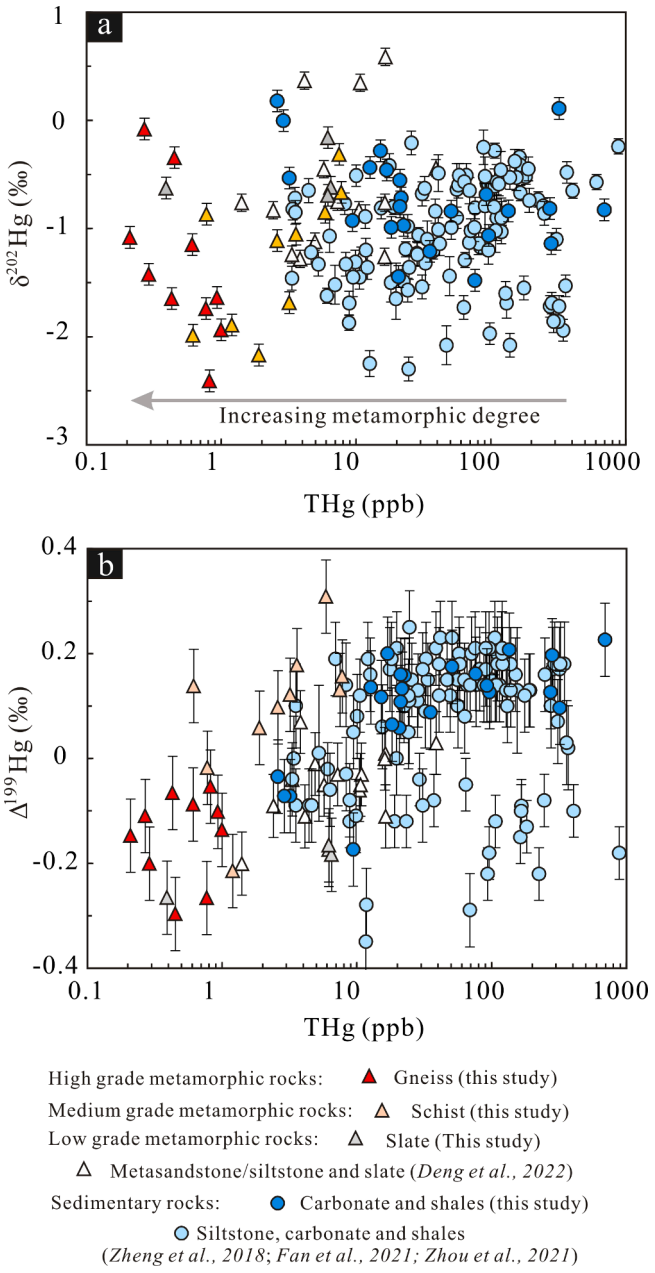

Fig. 5. (a) THg vs. δ^{202}Hg and (b) THg vs. Δ^{199}Hg diagrams for Precambrian meta- and sedimentary rocks.

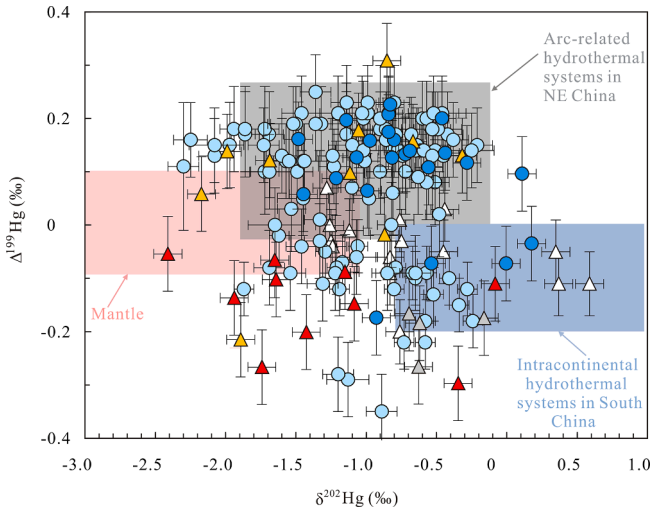

Fig. 6. Δ^{199}Hg versus δ^{202}Hg diagram, showing the Hg isotopic compositions of Precambrian meta- and sedimentary rocks worldwide and main Hg reservoirs in Earth. Area of arc-related hydrothermal system Hg is defined by Deng et al. (2021a, 2021b), intracontinental hydrothermal system Hg is that defined by Yin et al. (2019), Fu et al., 2020 and Deng et al. (2022), and estimated mantle Hg is defined by isotopic data of basalts and ordinary chondrites from Meier. (2016), and Moynier et al. (2020, 2021). Legends are the same as in Fig. 5.

and schist samples from the Xinghuadukou Group, slate from the Seluohe Group, gneiss from the Jiapigou Group and carbonate rocks from the Changcheng system show negative Δ^{199}Hg values (–0.30 to –0.03‰), similar to the terrestrial Hg signals (Fig. 3). The graphite schists from the Mashan Group and sedimentary rocks from the Doushantuo Formation have positive Δ^{199}Hg values (0.06 to 0.31‰), compared well with the marine Hg signals (Fig. 3). All the studied samples show a positive linear correlation between Δ^{199}Hg and Δ^{201}Hg with $\Delta^{199}Hg/\Delta^{201}Hg$ ratio of 0.93 (n = 47; R^2 = 0.82) (Fig. 4).

5. Discussion

5.1. Loss of Hg during the Precambrian basement metamorphism

As a chalcophile element, super enrichment of Hg (up to hundreds of ppm) was commonly observed in the low-temperature hydrothermal systems (Deng et al., 2021a and reference therein) and sulfide-bearing sedimentary rocks (Shen et al., 2019, 2020). Due to the affinity of Hg to organic material in sediments, organic-rich sedimentary rocks (e.g., black shales) should be more enriched in Hg than low-organic sedimentary rocks (e.g., carbonates, sandstones). Given the absence of abundant sulfides in the studied rocks, the higher Hg contents in black shales in the Doushantuo Formation (243 ± 209 ppb, 1SD, n = 8), compared to that in limestone and dolostone samples in the Doushantuo Formation (25.6 ± 17.8 ppb, 1SD, n = 11) and Gaoyuzhuang Formation (4.54 ± 3.24 ppb, 1SD, n = 4), are likely caused by their higher organic matter contents.

Metamorphosed sedimentary rocks show lower Hg concentrations than un-metamorphosed sedimentary rocks. For instance, graphite schist samples show Hg contents of 4.1 ± 2.6 ppb (1SD, n = 8), even their total organic carbon contents are up to 30 wt% (Li et al., 2008). High-grade metamorphic rocks, such as gneiss from the Xinghuadukou and Jiapigou Formations, show Hg contents of < 1 ppb. The medium-grade metamorphic schist samples have Hg contents (0.62–7.80 ppb) similar to the slate samples from the Seluohe Formation (0.39–6.50 ppb), but lower than the low-grade metasedimentary rocks (slate and metasandstone) in South China (Fig. 5; 1.40–38.7 ppb; Deng et al., 2022). The low abundance of Hg in metamorphic rocks suggests the loss of Hg during metamorphism. With the increase of burial depth, the grades of metamorphism are increased by increasing temperature. This could cause the loss of Hg due to the thermal sensibility of Hg and its strong volatility at the high-temperature conditions (Smith et al., 2008; Meier et al., 2016). In addition, low Hg contents in the metamorphic rocks would be also caused by the post-metamorphic thermal flow offered by the underlying magmatism. For example, Hg in the intracontinental hydrothermal systems in the South China Craton was likely sourced from the Precambrian metamorphic rocks driven by the regional magmatism (Fu et al., 2020; Deng et al., 2022). Therefore, our data indicate extremely low Hg contents in Earth's crystalline basements given their main composition of high-medium grade metamorphic rocks.

5.2. Lack of systematic Hg-MDF during metamorphism?

Recent studies have made great progress in understanding the

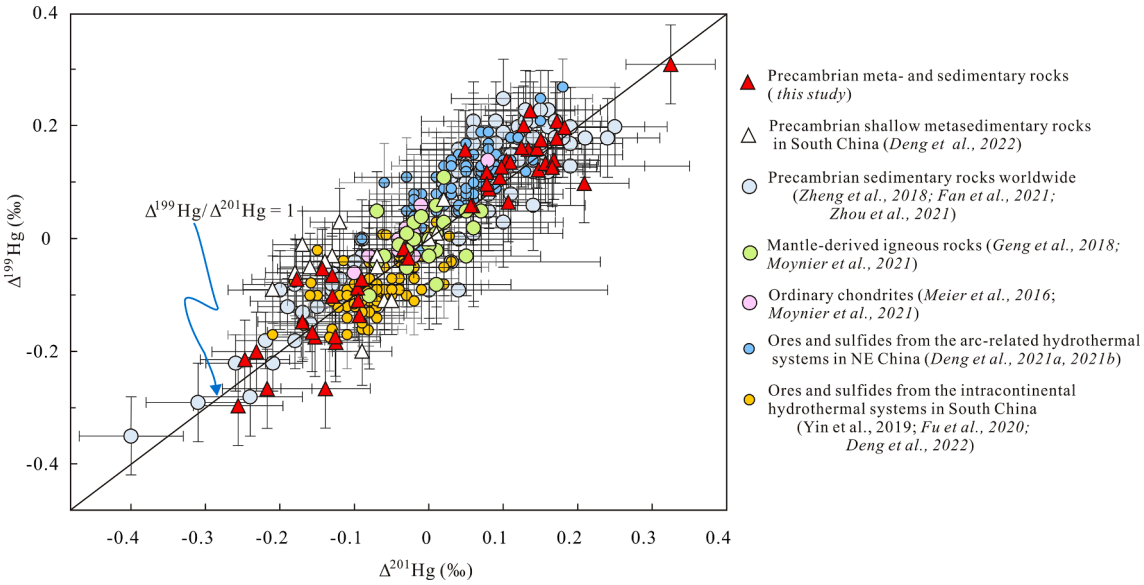

Fig. 7. Δ^{199}Hg versus Δ^{201}Hg diagram for rock and ore samples showing Δ^{199}Hg/Δ^{201}Hg of ~ 1.

isotopic composition of Hg in deep reservoirs (Fig. 6). Based on a few ^{3}He-rich basalts, Moynier et al. (2021) proposed that the primitive mantle has negative δ^{202}Hg values of −1.7 ± 0.6‰ (1SD). Arc-related hydrothermal deposits and igneous rocks containing recycled Hg from the oceanic crust mostly show negative δ^{202}Hg values (Deng et al., 2021a, b; Wang et al., 2021). Intracontinental hydrothermal deposits mainly show positive δ^{202}Hg values (Yin et al., 2019; Fu et al., 2020; Deng et al., 2021a, 2022). Our study shows that the Precambrian metamorphic and sedimentary rocks mostly show negative δ^{202}Hg values (Fig. 5). Significantly, the lack of correlation between δ^{202}Hg and metamorphic grade ($p > 0.05$, T-test) and the similar δ^{202}Hg values between metamorphic and sedimentary rocks ($p > 0.05$, ANOVA), suggest no systematic Hg-MDF during the metamorphism.

Hg-MDF occurs during a large number of geophysical and geochemical processes at low-temperature conditions (Blum et al., 2014 and references therein). Given δ^{202}Hg values of sedimentary rocks is complicated by various Hg-MDF processes during sedimentation and diagenesis, it is unrealistic to decipher the Hg-MDF during metamorphism simply by comparing δ^{202}Hg between the metamorphic and sedimentary rocks in our study. More experimental work is needed to reveal the Hg-MDF during metamorphism.

5.3. No significant Hg-MIF during the metamorphism

Unlike Hg-MDF, Hg-MIF occurs mainly during photochemical reactions (Blum et al., 2014). The Δ^{199}Hg/Δ^{201}Hg ratio of ~ 1 for the studied samples (Fig. 4) is consistent with that observed during aqueous Hg(II) photoreduction (Bergquist and Blum, 2007). Photochemical processes result in positive Δ^{199}Hg values in the atmospheric Hg(II) and negative Δ^{199}Hg values in gaseous Hg(0) (Bergquist and Blum, 2007). Atmospheric Hg(II) species are water-soluble and readily deposited into the ocean via wet deposition (Rolison et al., 2013; Štrok et al., 2015), whereas gaseous Hg(0) is preferentially uptaken by vegetation and deposited to soil via litterfall (Biswas et al., 2008; Demers et al., 2013). For this reason, marine sediments and coastal sediments are characterized by positive and negative Δ^{199}Hg, respectively (Blum et al., 2014), due to offshore and nearshore regions mainly receiving Hg via atmospheric Hg(II) deposition and soil erosion, respectively (Yin et al., 2015).

In this study, black shales from the Doushantuo Formation display positive Δ^{199}Hg values (0.16 ± 0.09‰; n = 8; 2SD), consistent with their basinal deposition origin. Positive Δ^{199}Hg values (0.06–0.31‰) were observed in the graphite schist samples from the Mashan Group (Fig. 2). The δ^{13}C values of these graphite samples (–32.1 to −16.8‰) suggest a marine plant source for their protolith (Li et al., 2008). Mercury in marine organisms is generally characterized by positive Δ^{199}Hg values due to the absorption of atmospheric Hg(II) from seawater (Blum et al., 2014). Therefore, positive Δ^{199}Hg values in the graphite schists could share a similar Hg source to normal marine sediments, which mainly receive seawater Hg (mainly consists of atmospheric Hg(II) species) via organic matter shuttle (Grasby et al., 2019). Given the similar positive Δ^{199}Hg values between the metamorphic rocks and their proposed marine protoliths, we infer no significant Hg-MIF occurred during metamorphism.

The lack of Hg-MIF during metamorphism can also be supported by our results on metamorphosed and un-metamorphosed coastal sedimentary rocks. As shown in Fig. 2, gneiss samples from the Xinghuadukou and Jiapigou groups, slate from the Seluohe Group, and dolomite and limestone from the Changcheng system show significant negative Δ^{199}Hg values (-0.30 to −0.02‰) similar to modern soil. As mentioned above, the protoliths of the Precambrian metamorphic rocks with negative Δ^{199}Hg values are pelites and clastic rocks sourced from the continental materials at the continental margin setting. Modern continental weathering materials (e.g., soil) show negative Δ^{199}Hg values (Biswas et al., 2008; Demers et al., 2013). Although plant cover prior to the Cambrian was limited (Rubinstein et al., 2010; Leliaert et al., 2012; Lenton et al., 2016), a recent study by Zarsky et al. (2021) suggested the expansion of the first terrestrial flora during the Proterozoic period. Based on the negative Hg-MIF signals in the Mesoproterozoic coastal sedimentary rocks in this study, we suggest that early terrestrial flora may have uptaken large amounts of atmospheric Hg(0) into the terrestrial soil, similar to the role of modern vegetation and soil as a major sink atmospheric Hg(0). Additionally, the negative Hg-MIF signals also could be caused by photoreduction of Hg(II) complexed by reduced sulfur ligands and/or enhanced sequestration of atmospheric Hg(0) to the sediments by thiols and sulfide that were enriched in the surface ocean (Zheng et al., 2018). Other mechanisms for the deposition of Hg(0) in the terrestrial systems cannot be precluded, but more experimental works are needed. Nevertheless, negative Δ^{199}Hg values in the Precambrian rocks indicate the existence of a complementary Hg reservoir for the positive Δ^{199}Hg values in the Precambrian marine sediments.

6. Conclusions and implications

Our results on metamorphic rocks, combined with previous results on igneous and metamorphic rocks as well as hydrothermal ore deposits (Fig. 7), show large Hg-MIF signals with $\Delta^{199}Hg/\Delta^{201}Hg$ ratio of ~ 1.0, suggesting a broad existence of Hg-MIF signals in Earth's lithosphere. These Hg-MIF signals are related to Hg(II) photoreduction on Earth's surface and fit well with that observed in surface reservoirs (e.g., ocean and land). Sedimentation, magmatism, metamorphism and hydrothermal processes do not trigger Hg-MIF (Geng et al., 2018; Grasby et al., 2019; Moynier et al., 2021; Deng et al., 2021 and reference therein; This study). Therefore, any observed Hg-MIF signals in rocks and ore deposits (Fig. 7) should be sourced from Earth's surface reservoirs. For instance, recent studies observed a large variation of $\Delta^{199}Hg$ values in low-temperature hydrothermal systems (−0.3 to 0.4‰; Deng et al., 2021a and reference therein), which have been attributed to recycling of Hg via plate subduction or remobilization of the Precambrian basement (Fu et al., 2020; Deng et al., 2021a, 2022). Recent studies also observed pronounced Hg-MIF signals in global basalts (Moynier et al., 2020, 2021; Wang et al., 2021; Yin et al., 2022), suggesting recycling of crustal-derived Hg into the mantle.

Hg in the primitive mantle has $\Delta^{199}Hg$ values of ~ 0‰ (Moynier et al., 2021), which are distinct from the significant $\Delta^{199}Hg$ values in the Precambrian rocks (−0.4 to 0.3‰; Fu et al., 2020; Fan et al., 2021; Cabral et al., 2022; Deng et al., 2021a, 2022 and this study). Due to its unique solution, Hg-MIF signals can be used to trace crustal-mantle interactions and crustal material recycling, which are extensively occurring in Earth's interior due to the relentless geological processes, such as mantle magma upwelling, ancient crustal delamination and crustal plate subduction.

This study characterizes the Hg-MIF signature in the Precambrian basement and proposes no Hg-MIF during metamorphism. Therefore, Hg-MIF signals can work as a tracer for Hg cycling in Earth's interior. It is worthy to mention that the significant loss of Hg during basement metamorphism would lead to the release of large amounts of Hg. The destination of these released Hg however remains unclear. Further work is required to investigate whether it goes to the atmosphere as gaseous Hg(0) or is involved in the hydrothermal systems as dissolved Hg(II).

Declaration of Competing Interest

The authors declare that they have no known competing financial interests or personal relationships that could have appeared to influence the work reported in this paper.

Acknowledgments

This study was supported by the National Natural Science Foundation of China (41873047, 41603020), the Croucher Chinese Visitorships from Croucher Foundation and the Research Matching Grant (185219) from Lingnan University. Anzong Fu and Sheng Lu are thanked for their help during fieldwork.

Appendix A. Supplementary data

Supplementary Table Hg contents and isotopic compositions of the Precambrian and standard samples of this study. Supplementary data to this article can be found online at https://doi.org/10.1016/j.precamres.2022.106646.

References

Ader, M., Thomazo, C., Sansjofre, P., Busigny, V., Papineau, D., Laffont, R., Cartigny, P., Halverson, G.P., 2016. Interpretation of the nitrogen isotopic composition of Precambrian sedimentary rocks: Assumptions and perspectives. Chem. Geol. 429, 93–110.

Bauluz, B., Mayayo, M.J., Fernandez-Nieto, C., Lopez, J.M.G., 2000. Geochemistry of Precambrian and Paleozoic siliciclastic rocks from the Iberian Range (NE Spain): Implications for source-area weathering, sorting, provenance, and tectonic setting. Chem. Geol. 168, 135–150.

Bergquist, B.A., Blum, J.D., 2007. Mass-dependent and -independent fractionation of hg isotopes by photoreduction in aquatic systems. Science 318 (5849), 417–420.

BGMRHP (Bureau of Geology and Mineral Resources of Heibei Province), 1989. Regional Geology of Heibei Province, Beijing Municipality and Tianjin Municipality. Geological Publishing House: Beijing, 1–741.

BGMRJP (Bureau Geology and Mineral Resources of Jilin Province), 1988. Regional Geology of Jilin Province. Geological Publishing House: Beijing, 1-114.

Biswas, A., Blum, J.D., Keeler, G.J., 2008. Mercury storage in surface soils in a central Washington forest and estimated release during the 2001 Rex Creek Fire. Sci. Total Environ. 404 (1), 129–138.

Blum, J.D., Bergquist, B.A., 2007. Reporting of variations in the natural isotopic composition of mercury. Analyt. Bionalyt. Chem. 388 (2), 353–359.

Blum, J.D., Sherman, L.S., Johnson, M.W., 2014. Mercury Isotopes in Earth and Environmental Sciences. Annu. Rev. Earth Pl. Sc. 42 (1), 249–269.

Cabral, A.R., Deng, C.Z., Yin, R.S., Yakubovich, O.V., Stuart, F.M., Tupinamba, M., Lehmann, B., 2022. Metal recycling tracked by mercury and helium isotopes in platnum-palladium nuggets from Corrego Bom Sucesso. Brazil. Chem. Geol. 593, 120752.

Chen, J.B., Hintelmann, H., Zheng, W., Feng, X.B., Cai, H.M., Wang, Z.H., Yuan, S.L., Wang, Z.W., 2016. Isotopic evidence for distinct sources of mercury in lake waters and sediments. Chem. Geol. 426, 33–44.

Condie, K.C., 1990. Growth and accretion of continental crust: Inferences based on Laurentia. Chem. Geol. 83 (3-4), 183–194.

Dasgupta, S., Raith, M.M., Sarkar, S., 2008. New perspectives in the study of the Precambrian continental crust of India: An integrated sedimentologic, isotopic, tectonometamorphic and seismological appraisal. Precambrian Res. 162, 1–3.

Demers, J.D., Blum, J.D., Zak, D.R., 2013. Mercury isotopes in a forested ecosystem: Implications for air-surface exchange dynamics and the global mercury cycle. Global Biogeochem. Cy. 27 (1), 222–238.

Deng, C.Z., Li, C.L., Rong, Y.M., Chen, D., Zhou, T., Wang, X.Y., Chen, H.Y., Lehmann, B., Yin, R.S., 2021a. Different metal sources in the evolution of an epithermal ore system: Evidence from mercury isotopes associated with the Erdaokan epithermal Ag-Pb-Zn deposit. NE China. Gondwana Res. 95, 1–9.

Deng, C.Z., Sun, G.Y., Rong, Y.M., Sun, R.Y., Sun, D.Y., Lehmann, B., Yin, R.S., 2021b. Recycling of mercury from the atmosphere-ocean system into volcanic-arc-associated epithermal gold systems. Geology 49, 309–313.

Deng, C., Zhang, J., Hu, R., Luo, K., Zhu, Y., Yin, R., 2022. Mercury isotope constraints on the genesis of Late Mesozoic Sb deposits in South China. Sci. China Earth Sci. 65 (2), 269–281.

Fan, H.F., Fu, X.W., Ward, J.F., Yin, R.S., Wen, H.J., Feng, X.B., 2021. Mercury isotopes track the cause of carbon perturbations in the Ediacaran Ocean. Geology 49, 248–252.

Fu, S., Hu, R., Yin, R., Yan, J., Mi, X., Song, Z., Sullivan, N.A., 2020. Mercury and in situ sulfur isotopes as constraints on the metal and sulfur sources for the world's largest Sb deposit at Xikuangshan, Southern China. Miner. Deposita 55 (7), 1353–1364.

Geng, H., Yin, R., Li, X., 2018. An optimized protocol for high precision measurement of Hg isotopic compositions in samples with low concentrations of Hg using MC-ICP-MS. J. Analyt. Atom. Spectrom. 33 (11), 1932–1940.

Grasby, S.E., Shen, W., Yin, R., Gleason, J.D., Blum, J.D., Lepak, R.F., Hurley, J.P., Beauchamp, B., 2017. Isotopic signatures of mercury contamination in latest Permian oceans. Geology 45 (1), 55–58.

Grasby, S.E., Them, T.R., Chen, Z., Yin, R., Ardakani, O.H., 2019. Mercury as a proxy for volcanic emissions in the geologic record. Earth Sci. Rev. 196, 102880.

Gratz, L.E., Keeler, G.J., Blum, J.D., Sherman, L.S., 2010. Isotopic composition and fractionation of mercury in Great Lakes precipitation and ambient air. Environ. Sci. Technol. 44 (20), 7764–7770.

Leliaert, F., Smith, D.R., Moreau, H., Herron, M.D., Verbruggen, H., Delwiche, C.F., De Clerck, O., 2012. Phylogeny and molecular evolution of the green algae. Crit. Rev. Plant Sci. 31 (1), 1–46.

Lenton, T.M., Dahl, T.W., Daines, S.J., Mills, B.J.W., Ozaki, K., Saltzman, M.R., Porada, P., 2016. Earliest land plants created modern levels of atmospheric oxygen. Proc. Natl. Acad. Sci. U. S. A. 113 (35), 9704–9709.

Li, C.D., Zhang, F.Q., Miao, L.C., Xie, H.Q., Hua, Y.Q., Xu, Y.W., 2007. Reconsideration of the Seluohe Group in Seluohe area, Jilin Province. J. Jilin U. (Earth Sci. Ed.) 37, 841–847 in Chinese with English abstract.

Li, G.H., Huang, Y.W., Wu, R.T., Xu, D.J., 2008. Origin of carbon and concentration of uranium and vanadium from Liumao graphite formation in Jixi. Glob. Geol 27, 19–22 in Chinese with English abstract.

Long, X., Xu, B., Yuan, C., Zhang, C., Zhang, L., 2019. Precambrian crustal evolution of the southwestern Tarim Craton, NW China: Constraints from new detrital zircon ages and Hf isotopic data of the Neoproterozoic metasedimentary rocks. Precambrian Res. 334, 105473.

McFadden, K.A., Huang, J., Chu, X., Jiang, G., Kaufman, A.J., Zhou, C., Yuan, X., Xiao, S., 2008. Pulsed oxidation and biological evolution in the Ediacaran Doushantuo Formation. Proc. Natl. Acad. Sci. U. S. A. 105 (9), 3197–3202.

Meier, M.M.M., Cloquet, C., Marty, B., 2016. Mercury (Hg) in meteorites: Variations in abundance, thermal release profile, mass-depedent and mass-independent isotopic fractionation. Geochim. Cosmochim. Ac. 182, 55–72.

Meng, M., Sun, R.-y., Liu, H.-W., Yu, B., Yin, Y.-G., Hu, L.-G., Shi, J.-b., Jiang, G.-B., 2019. An integrated model for input and migration of mercury in Chinese coastal sediments. Environ. Sci. Technol. 53 (5), 2460–2471.

Miao, L.C., Liu, D.Y., Zhang, F.Q., Fan, W.M., Shi, Y.R., Xie, H.Q., 2008. Zircon SHRIMP U-Pb ages of the "Xinghuadukou Group" in Hanjiayuanzi and Xinlin areas and the "Zhalantun Group" in Inner Mongolia, Da Hinggan Mountains. Chinese Sci. Bull. 52, 1112–1124.

Moynier, F., Chen, J., Zhang, K.e., Cai, H., Wang, Z., Jackson, M.G., Day, J.M.D., 2020. Chondritic mercury isotopic composition of Earth and evidence for evaporative equilibrium degassing during the formation of eucrites. Earth Planet. Sci. Lett. 551, 116544.

Moynier, F., Jackson, M.G., Zhang, K.e., Cai, H., Halldórsson, S.A., Pik, R., Day, J.M.D., Chen, J., 2021. The mercury isotopic composition of Earth's mantle and the use of mass independently fractionated Hg to test for recycled crust. Geophys. Res. Lett. 48 (17).

Rolison, J.M., Landing, W.M., Luke, W., Cohen, M., Salters, V.J.M., 2013. Isotopic composition of species-specific atmospheric Hg in a coastal environment. Chem. Geol. 336, 37–49.

Rubinstein, C.V., Gerrienne, P., de la Puente, G.S., Astini, R.A., Steemans, P., 2010. Early middle Ordovician evidence for land plants in Argentina (eastern Gondwana). New Phytol. 188 (2), 365–369.

Shen, J., Algeo, T.J., Chen, J.B., Planavsky, N.J., Feng, Q.L., Yu, J.X., Liu, J.L., 2019. Mercury in marine Ordovician/Silurian boundary sections of South China is sulfide-hosted and non-volcanic in origin. Earth Planet. Sci. Lett. 511, 130–140.

Shen, J., Feng, Q., Algeo, T.J., Liu, J., Zhou, C., Wei, W., Liu, J., Them, T.R., Gill, B.C., Chen, J., 2020. Sedimentary host phases of mercury (Hg) and implications for use of Hg as a volcanic proxy. Earth Planet. Sci. Lett. 543, 116333.

Shen, J., Yin, R.S., Zhang, S., Algeo, T.J., Bottier, D.J., Yu, J.X., Xu, G.Z., Penman, D., Wang, Y.D., Li, L.Q., Shi, X., Planavsky, N.J., Feng, Q.L., Xie, S.C., 2022. Intensified continental chemical weathering and carbon-cycle perturbations linked to volcanism during the Triassic-Jurassic transition. Nat. Commun. 13, 299.

Sherman, L.S., Blum, J.D., Keeler, G.J., Demers, J.D., Dvonch, J.T., 2012. Investigation of local mercury deposition from a coal-fired power plant using mercury isotopes. Environ. Sci. Technol. 46 (1), 382–390.

Sherman, L.S., Blum, J.D., Nordstrom, D.K., McCleskey, R.B., Barkay, T., Vetriani, C., 2009. Mercury isotopic composition of hydrothermal systems in the Yellowstone Plateau volcanic field and Guaymas Basin sea-floor rift. Earth Planet. Sci. Lett. 279 (1-2), 86–96.

Smith, C.N., Kesler, S.E., Blum, J.D., Rytuba, J.J., 2008. Isotope geochemistry of mercury in source rocks, mineral deposits and spring deposits of the California Coast Ranges, USA. Earth Planet. Sci. Lett. 269 (3-4), 399–407.

Sonke, J.E., 2011. A global model of mass independent mercury stable isotope fractionation. Geochem. Cosmochim. Ac. 75 (16), 4577–4590.

Štrok, M., Baya, P.A., Hintelmann, H., 2015. The mercury isotope composition of Arctic coastal seawater. C. R. Geosci. 347 (7-8), 368–376.

Tang, Y.Y., Bi, X.W., Yin, R.S., Feng, X.B., Hu, R., 2017. Concentrations and isotopic variability of mercury in sulfifide minerals from the Jinding Zn-Pb deposit, Southwest China. Ore Geol. Rev. 90, 958–969.

Wang, X., Deng, C., Yang, Z., Zhu, J.-J., Yin, R., 2021. Oceanic mercury recycled into the mantle: Evidence from positive δ199Hg in lamprophyres. Chem. Geol. 584, 120505.

Ward, J.F., Verdel, C., Campbell, M.J., Leonard, N., Duc Nguyen, A.i., 2019. Rare earth element geochemistry of Australian Neoproterozoic carbonate: Constraints on the Neoproterozoic oxygenation events. Precambrian Res. 335, 105471.

Wu, G., Chen, Y.C., Chen, Y.J., Zeng, Q.T., 2012. Zircon U-Pb ages of the metamorphic supracrustal rocks of the Xinghuadukou Group and granitic complexes in the Argun massif of the northern Great Hinggan Range, NE China, and their tectonic implications. J. Asian Earth Sci. 49, 214–233.

Xu, C., Yin, R., Peng, J., Hurley, J.P., Lepak, R.F., Gao, J., Feng, X., Hu, R., Bi, X., 2018. Mercury isotope constraints on the source for sediment-hosted lead-zinc deposits in the Changdu area, southwestern China. Miner. Deposita 53 (3), 339–352.

Xu, J.L., 2018. Metamorphism of the Xinghuadukou Complex in the Erguna. Jilin University, Changchun, pp. 1–154. Ph.D Thesis.

Yin, R.S., Chen, D., Pan, X., Deng, C.Z., Chen, L.M., Song, X.Y., Yu, S.Y., Zhu, C.W., Wei, X., Xu, Y., Feng, X.B., Blum, J.D., Lehmann, B., 2022. Mantle Hg isotopic heterogeneity and evidence of oceanic Hg recycling into the mantle. Nat. Commun. 13, 948.

Yin, R., Deng, C., Lehmann, B., Sun, G., Lepak, R.F., Hurley, J.P., Zhao, C., Xu, G., Tan, Q., Xie, Z., Hu, R., 2019. Magmatic-hydrothermal origin of mercury in Carlin-style and epithermal gold deposits in China: evidence from mercury stable isotopes. ACS Earth Space Chem. 3 (8), 1631–1639.

Yin, R., Feng, X., Chen, B., Zhang, J., Wang, W., Li, X., 2015. Identifying the sources and processes of mercury in subtropical estuarine and ocean sediments using Hg isotopic composition. Environ. Sci. Technol. 49 (3), 1347–1355.

Yin, R., Krabbenhoft, D.P., Bergquist, B.A., Zheng, W., Lepak, R.F., Hurley, J.P., 2016. Effects of mercury and thallium concentrations on high precision determination of mercury isotopic composition by Neptune Plus multiple collector inductively coupled plasma mass spectrometry. J. Analyt. Atomic Spectrometry 31 (10), 2060–2068.

Zarsky, J.D., Zarsky, V., Hanacek, M., Zarsky, V., 2021. Cryogenian glacial habitats as a plant terrestrialisation cradle-the origin of the anydrophytes and Zygnematophyceae split. EcoEvoRxiv. https://doi.org/10.32942/osf.io/t7h69.

Zerkle, A.L., Yin, R.S., Chen, C.Y., Li, X.D., Izon, G.J., Grasby, S.E., 2020. Anomalous fractionation of mercury isotopes in the Late Archean atmosphere: Nat. Commun. 11, 1709.

Zhao, G., Sun, M., Wilde, S.A., Sanzhong, L.i., 2005. Late Archean to Paleoproterozoic evolution of the North China Craton: key issues revisited. Precambrian Res. 136 (2), 177–202.

Zhao, G., Sun, M., Wilde, S.A., Li, S., 2004. A Paleo-Mesoproterozoic supercontinent: assembly, growth and breakup. Earth-Sci. Rev. 67 (1-2), 91–123.

Zheng, W., Gilleaudeau, G.J., Kah, L.C., Anbar, A.D., 2018. Mercury isotope signatures record photic zone euxinia in the Mesoproterozoic ocean. Proc. Natl. Acad. Sci. U. S. A. 115 (42), 10594–10599.

Zheng, Y.-F., Xiao, W.-J., Zhao, G., 2013. Introduction to tectonics of China. Gondwana Res. 23 (4), 1189–1206.

Zhou, T., Pan, X., Sun, R., Deng, C., Shen, J., Kwon, S.Y., Grasby, S.E., Xiao, J., Yin, R., 2021. Cryogenian interglacial greenhouse driven by enhanced volcanism: Evidence from mercury records. Earth Planet. Sci. Lett. 564, 116902.